Microwave-cavity-mode optimization by background antiresonance tuning

Michael T. Hatzon, Eugene N. Ivanov, Jeremy F. Bourhill, Maxim Goryachev, and Michael E. Tobar*

Quantum Technologies and Dark Matter Research Laboratory, Department of Physics, University of Western Australia, 35 Stirling Highway, Crawley, Western Australia 6009, Australia

(Received 22 April 2024; accepted 28 June 2024; published 30 July 2024)

To derive the best oscillator phase noise when implementing a high-Q resonator, the resonant spectral line shape must have high contrast and symmetry. Ideally, this line shape is second order and Lorentzian; however, in a high-mode-density spectral region, low-Q background spurious modes interact and distort the resonance. For a sapphire-loaded cavity resonator operating with whispering-gallery modes confined within the sapphire crystal, we show that this high contrast and symmetry can be achieved by meticulously changing the dimensions of the surrounding metallic cavity shield to tune the background low-Q structures into antiresonance. This works because the high-Q resonances are primarily defined by the sapphire, while the background modes are defined by the cavity shield. Alternatively, it has been shown that a similar result can be achieved by exciting the high-Q resonator with a balanced microwave dipole probe in a Mach-Zehnder interferometric configuration. The probe has been constructed from two separate coaxial electric field probes symmetrically inserted into a cylindrical-cavity resonator, from opposite sides with a small gap between them, so they can behave like an active wire-dipole antenna. The power into the two separate probes may be matched with an external variable attenuator in one of the arms of the interferometer. Conversely, the phase between the two electric field probes may be changed with an external variable phase shifter, which changes the nature of the field components to which the probe couples. The probe couples to the high-Q resonant modes as well as low-Q background modes, which can be made resonant or antiresonant with respect to the high-Q modes by changing this external phase. When the background modes are in antiresonance, the line shape of the high-Q mode can be made symmetric and with higher contrast. This technique has been applied to both whispering-gallery sapphire modes, as well as hollow-cavity resonators, without changing the dimensions of the cavity.

DOI: 10.1103/PhysRevApplied.22.014081

I. INTRODUCTION

High-precision low-phase-noise frequency sources are extremely important in a range of modern applications, from fundamental tests of physics [1–7], low-noise measurements [8], through digital communications, navigation, and radar technology to audio processing [9]. Amongst the best is the low-noise sapphire oscillator, both cryogenic (which implements Pound frequency stabilization) [10–13] and room temperature (which implements interferometric signal processing for frequency stabilization) [14–17]. Low-phase-noise resonator-oscillators operate optimally when configured with high-Q resonators with perfectly symmetric line shape, usually of Lorentzian form, so the phase noise will be filtered optimally outside the bandwidth of the resonator [18]. It has been shown that any asymmetry, such as a Fano-type asymmetry [19], will cause the phase noise of an oscillator to be enhanced [7,18].

The fact that microwave cavities are multimode devices, with probes that couple energy in and out of the cavity, means that high-Q modes exist amongst a background of low-Q modes with significant off-resonance transmission. These low-Q modes also couple to the external probing circuit, often acting to distort the operational modes with a more general Fano-type line shape [20]. An antiresonance is defined by a spectral location at which the destructive interference between an external driving force and a resonant mode, or multiple modes, results in a local minimum amplitude of oscillation. Previous work has examined an antiresonance system to probe phase information due to the interference fields of an atom and external pumped fields [21], as well as similar interference effects in microwave-magnon systems [22]. Here, the effect is purely electromagnetic, showing interference effects between microwave modes similar to that described previously [20].

*Contact author: 22873723@student.uwa.edu.au, michael.tobar@uwa.edu.au

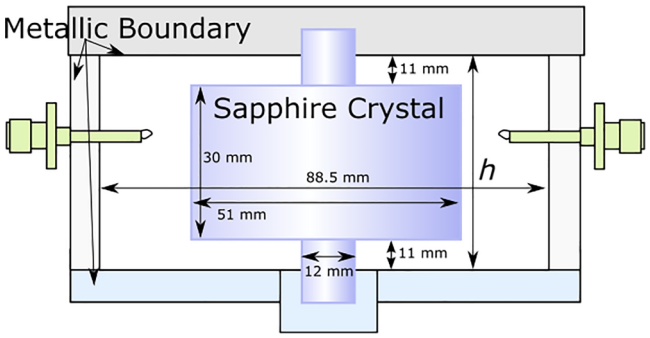

FIG. 1. The cryogenic sapphire-loaded cavity resonator. In this work, the height, h, of the cavity has been varied, which has tuned the background antiresonances without tuning the sapphire mode. In this work, $\Delta h = 0$ corresponds to a value of $h = 52.10$ mm.

In this work, we investigate ways for an operational high-Q mode to exist in a background antiresonance. In the first case, we examine a high-Q whispering-gallery (WG) mode sapphire-loaded cavity resonator cooled to near 4 K, as shown in Fig. 1. This type of resonator acts as the frequency determination for the highly stable cooled-sapphire oscillator, which may excite an atomic clock at the quantum projection noise limit [23]. For this case, we have succeeded in realizing the operation in a background antiresonance by modifying the dimensions of the copper cavity that surrounds it and we show that it optimizes the contrast and Q factor of the operational mode. Following this, we introduce the concept of a dipole-antenna probe with two input arms to excite the cavity resonator. The probing mechanism configuration is similar to a Mach-Zehnder interferometer [24], as the two arms may have the relative phase and amplitude varied. In this case, we show how it can be implemented to improve microwave lineshape symmetry and contrast simply through varying the external parameters. In this case, we have only undertaken measurements at room temperature as a proof-of-concept experiment.

II. QUANTIFYING SYMMETRY AND CONTRAST

Due to the importance of high contrast and symmetry for optimizing phase-noise performance, in this section the exact process of quantifying these values is described. The contrast values presented in this section and throughout this paper are calculated by fitting a parabola to the background of any narrow-span spectra acquired, where resonant modes or antiresonance features are removed from the data set. The maximum-decibel point of the experimental mode then has the corresponding value of the background at the same frequency subtracted off, to provide an estimated value of contrast.

The degree of symmetry of a mode, Σ, is determined from the transmission function (S_{12}), given by

$$\Sigma = \frac{\int_{-10\kappa_0}^{0} |S_{12}(f_0+f) - \beta_0 + S_{12}(f_0-f) - \beta_0| df}{\int_{-10\kappa_0}^{0} |S_{12}(f_0+f) - \beta_0| + |S_{12}(f_0-f) - \beta_0| df}, \tag{1}$$

where β_0 is the background term given by

$$\beta_0 = \frac{1}{2}(S_{12}(f_0 - 10\kappa_0) + S_{12}(f_0 + 10\kappa_0)), \tag{2}$$

in which κ_0 is the bandwidth of the mode (full width at half maximum). Here, f_0 is the frequency of the local maximum (or minimum for inversions). The integration region of ten bandwidths ($10\kappa_0$) is determined to sufficiently represent the mode structure. Since the vector network analyzer used in the measurements of $S_{12}(f)$ is digital with a set resolution bandwidth, the data have been interpolated and then integrated. The value of Σ provides a degree of mode symmetry, where an ideal Lorentzian (with Fano parameter $q = 0$) has a value of $\Sigma = 1$, corresponding to perfect symmetry, while perfect asymmetry will have a value of $\Sigma = 0$.

III. OPTIMIZING CONTRAST AND SYMMETRY OF A CRYOGENIC SAPPHIRE-LOADED CAVITY

We investigate background antiresonance tuning by changing the shield dimensions of a high-Q sapphire WG-mode resonator as shown in Fig. 1. High-quality-factor modes exist amongst background resonances and antiresonances. The key feature in this case is that the background antiresonances and resonances are tuned by varying the cavity height, h (dimension as shown in Fig. 2), while the high-Q resonances depend only on the crystal dimensions, as they are overwhelmingly located within the dielectric.

With each sequential change in the cavity height, a frequency shift in the relatively broad background modes has been observed, on the order of 30 kHz per micrometer for the change in cavity height. In this case, it has therefore been possible to shift an antiresonance directly onto the observed mode. As the background antiresonance has been tuned over the high-Q mode, distortion of the high-Q mode has been observed, with a large change in both contrast and symmetry. This effect may be explained by the onset of a Fano resonance, as seen in Fig. 2, modeled through a mutual resistive term between the two modes as described in Ref. [20]. This result has been reproduced with a second sapphire resonator at a similar antiresonance position, with the orientation of the sapphire chosen to maximize probe coupling to one of the doublets and minimize it to the other. The small finite coupling to the second under coupled mode causes some slight variations to the effect. These two resonators are being developed to create high-stability and

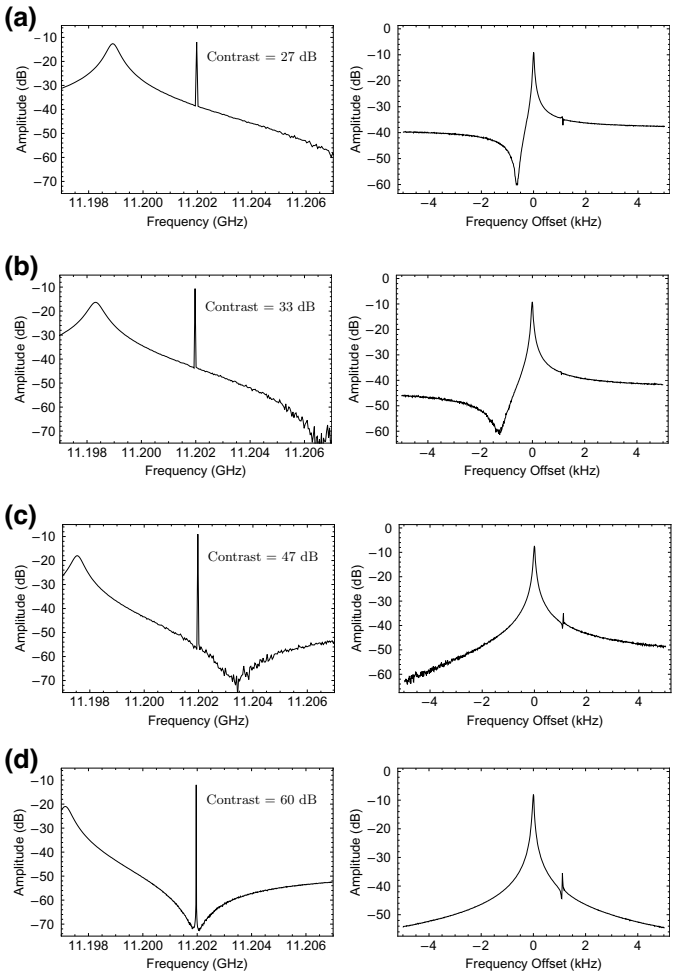

FIG. 2. The effect of changing the cavity shield dimensions on a high-Q sapphire fundamental quasi-TM $WGH_{16,0,0}$ mode centered at 11.202 GHz. Left-hand column, a 10-MHz span showing the properties of the background mode with contrast. Right-hand column, a 10-kHz span showing the properties of the high-Q mode. (a)–(d) A cylindrical shielding cavity height of (a) $h \approx 52.10$ mm, (b) $\Delta h \approx 60$ μm, (c) $\Delta h \approx 70$ μm, and (d) a further $\Delta h \approx 30$ μm. The bottom curve shows unambiguously that the best symmetry and contrast occur in a background antiresonance. Calculating the Q factors from Fano fits to the transmission curve leads to a maximum loaded Q factor of 2.5×10^8 in antiresonance; however, the value only deviates below this by no more than 20% across the antiresonance tuning range.

low-noise cryogenic sapphire oscillators [18,25], so it is important to gain good symmetry and contrast in order to achieve optimum phase-noise performance.

IV. WIRE-DIPOLE PROBE

To measure or excite a normal electric field, an electric field probe may be constructed from a 50-Ω open-end coaxial cable oriented in a parallel direction to this field, with the central conductor extruded directly out of the cable. Constructing an antenna that measures or excites

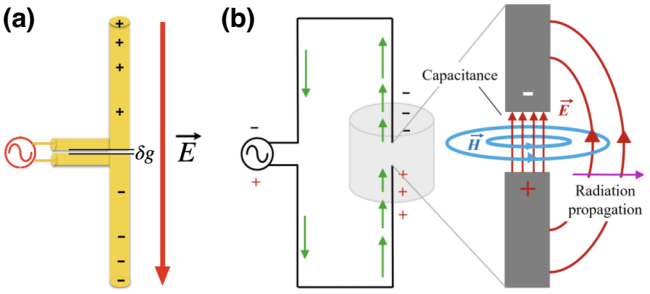

FIG. 3. (a) A dipole antenna driven by a voltage source through a subwavelength gap, so that the current and voltage across the antenna are out of phase and hence capacitive. Likewise, the near electric ($\vec{E}$) and magnetic ($\vec{H}$) fields are out of phase. (b) The modified dipole-antenna arrangement for use as a coupling probe to a cavity resonator (light-gray cylinder). On the right is an enlargement of the gap between the antenna arms, illustrating the capacitive coupling.

the tangential field is more complicated as, in principle, the tangential field goes to zero for a perfect conducting probe. However, this may be achieved by using a balanced wire-dipole probe, made with two noncontacting adjacent electric field probes, as shown in Fig. 3(a). The dipole antenna nominally consists of two wires with a subwavelength gap δg, through which the electric field is excited or measured. The gap is much smaller than the antenna dimensions and provides capacitive coupling.

To adapt this type of antenna to a cylindrical-cavity resonator, the probe may be coupled through the top and bottom of the cylinder as shown in Fig. 3(b), combined with a hybrid 180° junction or balun to balance the power and phase to the two arms of the dipole-probe antenna [26–30]. The phase and attenuation between the two adjacent coaxial cables of the dipole wire probe give extra degrees of freedom that may be varied while coupling to the modes of the resonator.

V. MICROWAVE DIPOLE-PROBE INTERFEROMETER

To use such a wire-dipole antenna to excite an empty cylindrical-cavity resonator, it has been set up symmetrically about the center of the cavity, as shown in Fig. 4, with the so-called top and bottom as depicted. Control over the phase and attenuation difference between the top and bottom antennas can be achieved by use of elements similar to a Mach-Zehnder interferometer [24] as shown in Fig. 5.

The antenna can produce dipole, monopole, or hybrid field patterns, as depicted in Fig. 6, determined by the phase difference $\Delta\phi = \phi_2 - \phi_1$ between the top and bottom probe. For a dipole configuration, we set to $\Delta\phi = \pi$. The depicted setup in Fig. 5 is in fact more general and allows $\Delta\phi$ to take any value between 0 and 2π. Two phase shifters combined in series after a 3-dB power splitter are

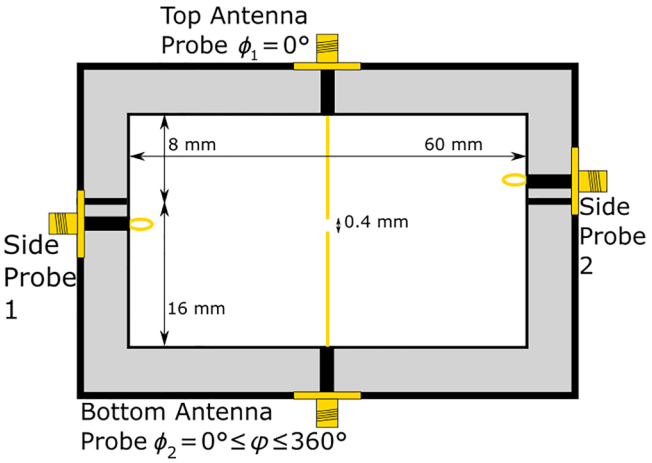

FIG. 4. The empty copper cylindrical cavity with dimensions and probe positions, with central conductors and SMA ports indicated in yellow.

necessary to ensure at least 2π phase shift in the frequency range of interest and utilize micrometers to vary the phase shift (line stretchers). Henceforth, relative phase variations

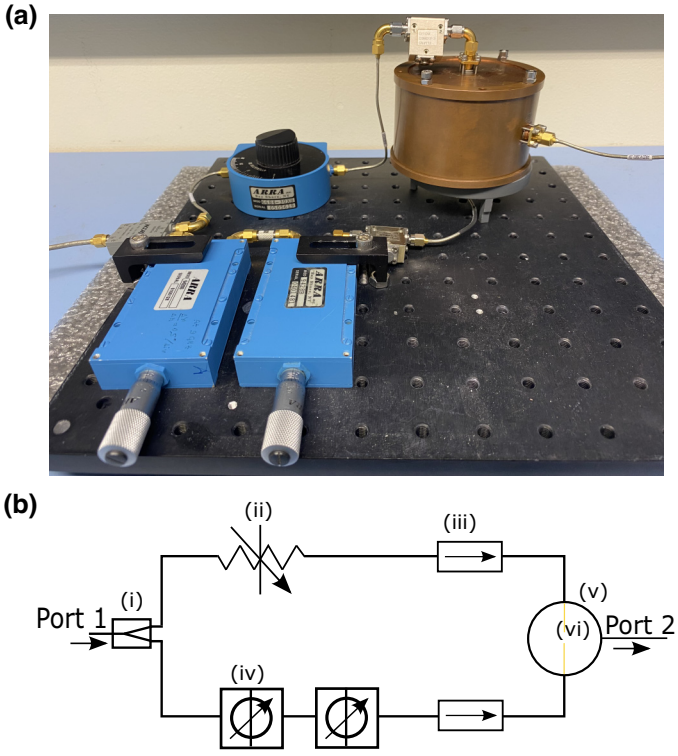

FIG. 5. (a) A photograph of the microwave interferometeric circuit. (b) A schematic illustrating the components: (i) power splitter, (ii) variable attenuator, (iii) isolator, (iv) phase shifter, (v) cavity resonator, and (vi) dipole wire probes. The setup is similar to a Mach-Zehnder interferometer, except that it measures resonance and antiresonance instead of bright and dark ports. For network-analyzer experiments, port 1 is labeled at the input of the interferometer, while probe 2 is labeled as the output probe on the side of the cavity.

in this work are stated in terms of millimeters. Due to the slight attenuation of these phase shifters, small variable and static attenuators have been used to balance out the attenuation in the arms of the interferometer. It is critical that both input probes of the cavity are at precisely the same power to ensure effectiveness of the dipole antenna as a function of $\Delta\phi$. Isolators are employed in each arm of the interferometer to function as a voltage-wave-standing-ratio- (VSWR) elimination mechanism. A VSWR causes reflections in the transmission lines and accentuates features of the circuit setup, rather than the dipole antenna. Thus it has been desirable that this VSWR should be eliminated.

As illustrated in Fig. 6, the introduction of a phase shift between the two dipole arms affects the orientation of the electric field to which the probe couples. This affects the coupling of the dipole probe to various cavity modes, dependent on the polarization of the mode, as well as the extent of the coupling to crosstalk [31,32] between the dipole probe and the output side probe. Antiresonances will form in such a system due to destructive interference between resonant modes and either the input driving field or the crosstalk; therefore, tuning the phase shift across the dipole probe can effectively change the spectral location and extent of destructive and constructive interference [33]. Thus, antiresonance and resonance frequencies may be tuned via the phase difference imposed by the interferometer. So, in contrast to the first method of tuning antiresonances by cavity height, this cavity-excitation method allows background antiresonances to be tuned by

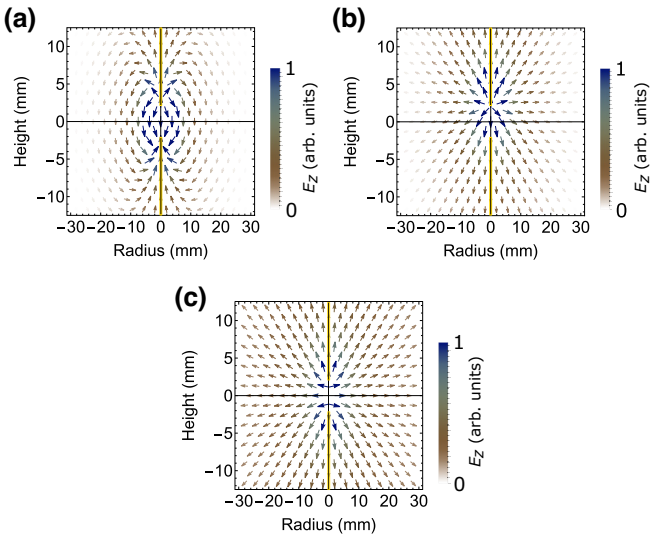

FIG. 6. The wire-dipole antenna can be configured to produce various electric field patterns, depending on the relative phase difference $\Delta\phi$ between the two arms. The three field configurations for a fixed time, t, are (a) dipole with $\Delta\phi = \pi$, (b) hybrid with $\Delta\phi = \pi/2$, and (c) monopole with $\Delta\phi = 0$, with probe positions drawn in yellow.

the nondestructive method of varying the phase difference between the input probe arms.

A. Operation and calibration of a cylindrical-cavity resonator

The configuration of the empty cylindrical-cavity resonator examined in this section is shown in Fig. 4. Unlike the sapphire-loaded cavity of Fig. 1, it is impossible to change the dimensions of a cavity resonator to tune the background modes without tuning the high-Q resonant mode itself, as it too is defined by the cavity dimensions.

Here, we examine the empty copper cylindrical-cavity resonator to gain an understanding of the transmission background coupled to the dipole interferometric antenna. Transmission spectra from 5 to 11 GHz are examined as the phase difference is varied, as shown in Fig. 7.

Two primary characteristics of the spectrum are (1) broad low-Q background resonances or antiresonances and (2) the appearance of sharp antiresonances. To deduce that the tuning of background resonances and antiresonances are in fact related to the phase shift inside the dipole-probe interferometer, one antenna arm has been deactivated by severe attenuation, while the other has been phase shifted and compared, when the attenuation has been set to zero, with the results plotted in Fig. 7. Deactivating one arm produces no phase-dependent effects, with three identical transmission spectra at different values of phase showing virtually no difference. On the contrary, with two active arms (attenuation set to zero), the dipole antenna produces significant changes in the spectra, particularly in the (9–10)-GHz region. This result suggests that frequency shifting of background resonances or antiresonances is caused by varying the phase difference ($\Delta\phi$) between the two arms of the active dipole antenna.

The use of the dipole probe in this manner allows for tuning of the background mode *without* frequency tuning the higher-Q mode. This allows similar control over the experiment without physically changing the cavity dimensions as in the prior case. In Fig. 8, we show the distinct interferometric pattern that gives rise to the tuning of the background resonances and antiresonances. This figure can also be used to calibration the sensitivity of the phase shifters. One can see that the operational modes have their best transmission properties when in a background

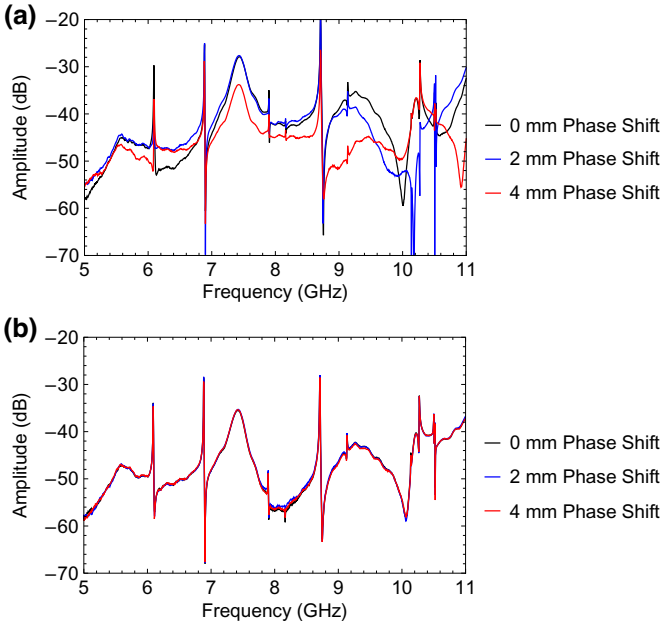

FIG. 7. The 8-GHz center transmission readout at three arbitrary equally spaced phase shifts with a span of 6 GHz. (a) The spectrum when the power in both arms of the interferometer driving the dipole antenna has no attenuation added (0 dB). (b) The spectrum when one arm of the interferometer driving the dipole antenna is attenuated by 30 dB, where the attenuation is controlled using the variable attenuator in Fig. 5. When both arms of the interferometer are activated, the appearance of broad and sharp antiresonances occur and can be seen in the (9–10)-GHz and (10–11)-GHz regions. When one arm is deactivated with 30-dB attenuation, the phase shift of the remaining interferometer arm makes no difference to the recorded spectrum, indicating that there is no more interference.

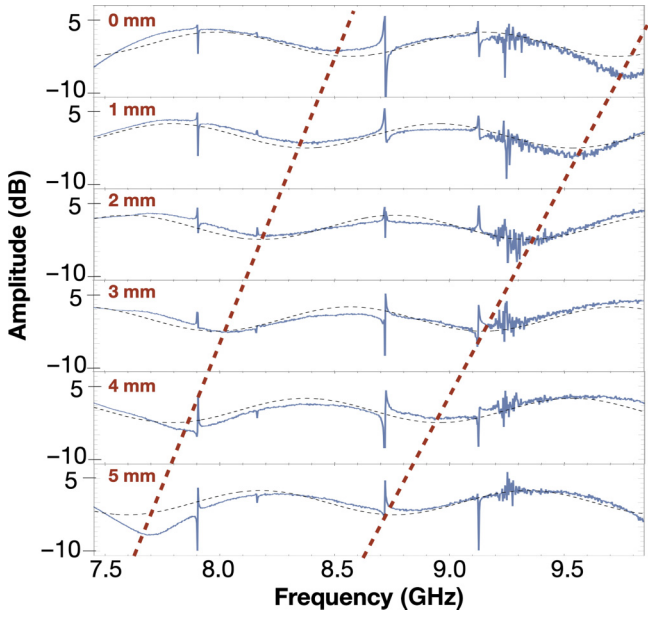

FIG. 8. The calibration graph for the frequency-dependent phase-shift measurements: six plots of S_{12} measurement data for each phase subtracted from the averaged transmission data across all six phases (0 mm to 5 mm in descending order). The black dashed line indicates a simple sinusoidal fit to help indicate the tuning of an antiresonance. The red dashed lines indicate the actual antiresonance tuning. These curves can be used to calibrate the frequency phase shift of the background modes. For example, at 8 GHz it roughly takes 4 mm of turning to go from resonance to antiresonance (approximately π phase shift).

antiresonance. In the next sections, we show that they have a better Q factor and contrast.

VI. DIPOLE INTERFEROMETRIC ANTENNA: CAVITY-MODE EXCITATION

A. Tuning a low-Q antiresonance

In Fig. 9, we show the tuning of a broad antiresonance by varying ($\Delta\phi$), with the effect of the antiresonances in proximity to the $TM_{1,1,0}$ 6.09 GHz mode shown at four unique positions.

The maximum mode symmetry in Fig. 9 (on antiresonance) has been achieved by tuning the broad antiresonance directly on to the mode of interest, done so by varying the phase of one of the antenna arms. There is also a significant increase in contrast of the mode with the background when this occurs, changing from a minimum contrast of 13 dB (antiresonance tuned away) to 20 dB (antiresonance tuned on to the mode). Tuning the antiresonance on to the mode of interest produces a higher degree of symmetry. The broad span in Fig. 9 on antiresonance helps to visualize this on a larger scale, where the mode of interest is now observed to be in the well of an antiresonance, with a lower-transmission background.

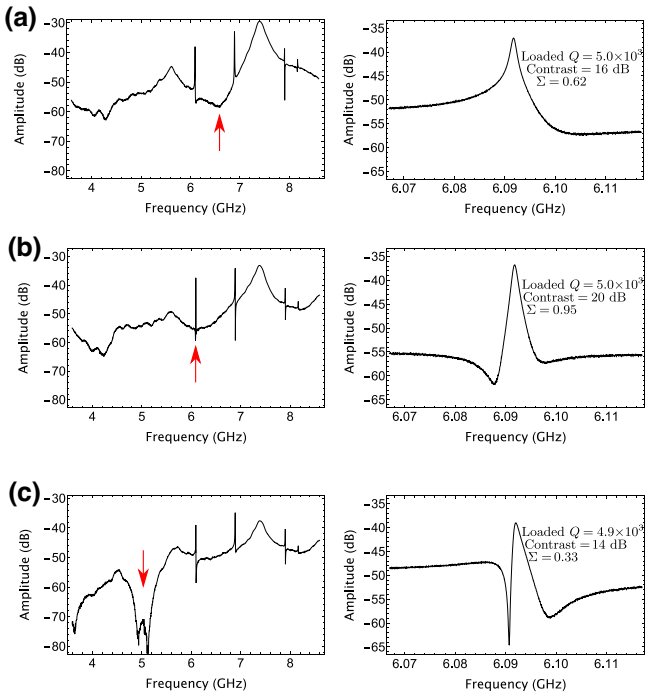

FIG. 9. A broad 5-GHz span (left-hand column) and a narrow 50-MHz span (right-hand column) of the $TM_{1,1,0}$ 6.09-GHz-mode transmission spectra at varying phase shift and constant attenuation. The mode is displayed when the antiresonance is positioned (a) to the right of the mode, (b) centrally on the mode, and (c) to the left of the mode. The antiresonance positions are indicated by a red arrow. The loaded Q, contrast, and symmetry values are given for the respective antiresonance positions.

B. Tuning a higher-Q antiresonance

Among the broad-tuning background antiresonances, there is also the presence of a few sharp or deeper antiresonances, similar to that observed in the cryogenic sapphire resonator in Sec. III. It has been possible to tune one of these sharp antiresonances to the same frequency of the 10.14-GHz mode. This leads to an optimization of contrast and symmetry shown in Fig. 10.

The contrast and symmetry are both maximized when the sharp antiresonance is positioned directly on the resonant mode center near 3-mm phase shift in this case, noting that the peak here is possibly underestimated due to the limited data resolution around this applied phase shift of the interferometer. The results show an increase of over 18 dB in contrast at the second point of maximum symmetry. Other high-symmetry peaks are also present in Fig. 10 as expected, which occurs when the background resonance is tuned to the $TM_{2,1,1}$ 10.14-GHz mode, but in such situations the contrast is poor due to the interference with the background resonance.

VII. DIPOLE INTERFEROMETRIC ANTENNA: SAPPHIRE WHISPERING-GALLERY-MODE EXCITATION

In this section, we show room-temperature results of when the dipole antenna is coupled to a high-Q sapphire whispering-gallery cavity as shown in Fig. 11, with similar supporting interferometric circuitry. These modes are more than an order of magnitude higher-Q than the empty copper-cavity modes. In this higher-Q system, several modes have been examined, which have displayed interesting behavior when tuning the phase of the interferometer.

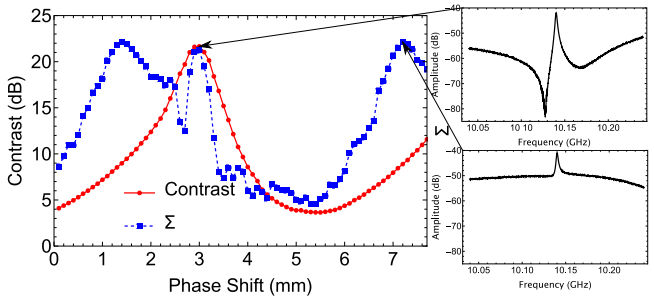

FIG. 10. The optimization of the 10.14-GHz mode when centered on antiresonance. The contrast (red, solid) and degree of symmetry, Σ (blue, squares) are plotted using a double y axis. The peak symmetry and contrast coincide near a 3-mm phase shift. The two local maximum transmission spectra are shown with their corresponding locations. The spectrum positioned in antiresonance has approximately 3 times better contrast. The Q factor of the mode is independent of the phase shift and equal to 4600.

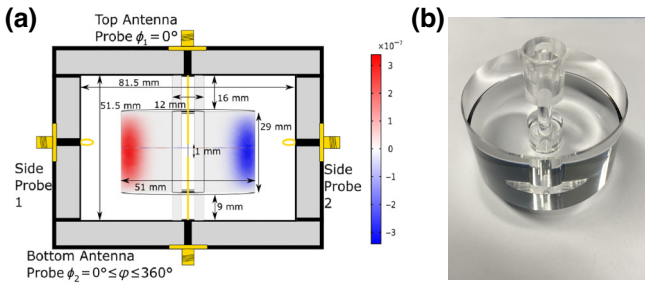

FIG. 11. (a) The copper cavity and the sapphire placed inside with the associated D_z field cross section for the $m = 11$ whispering-gallery mode. (b) A photograph of the sapphire with a cylindrical spindle. The gap between the dipole-antenna probes has been kept at around 1 mm for the sapphire cavity.

A. Tuning whispering-gallery mode type 1

The first WG mode analyzed is centered at 9.905 GHz, as shown in Fig. 12. From COMSOL finite-element modeling, we identify this mode as $WGH_{11,1,0}$. The results also show that the optimal symmetry and contrast occur when the operational mode is tuned within a background antiresonance. The contrast of the sapphire mode improves by several decibels, along with the line-shape symmetry when positioned on an antiresonance. Along with these results, a Q-factor increase of about 2% is observed. The effects of the side-probe coupling on the dipole tuning features of this mode have also been examined in Fig. 12.

The coupling data from Fig. 12 indicate less pronounced antiresonance effects at lower-output couplings when the contrast is low. When the probe is retracted, it is less coupled to the high-Q sapphire modes and detects less of this influence to background resonances. In contrast, when the output probe is near-unity coupled, the effects are more pronounced. To achieve good phase noise in an oscillator, high contrast is necessary and one usually designs the probes to be near-unity coupled.

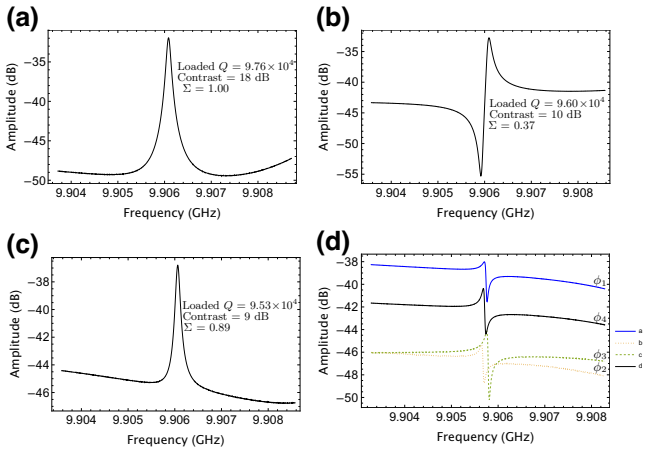

FIG. 12. The 9.905-GHz sapphire mode interacting with a background mode, with a narrow span (a) centered on the antiresonance, (b) with the antiresonance to the left of the mode, and (c) centered on the background resonance. Spectra (a)–(c) have the side probe coupling set to near 0.94, although the antiresonance-centered spectrum is slightly less coupled at 0.81. (d) Four transmission spectra in a low-coupled system with side-probe coupling near 0.1. Broadband transmission changes are observed for phase positions ϕ_1 to ϕ_4 and the ability to tune the broadband antiresonance is suppressed. The loaded Q, contrast, and symmetry values (Σ) are presented for each antiresonance position.

B. Tuning whispering-gallery mode type 2

The properties of tuning an antiresonance to the second high-Q sapphire mode are shown in Fig. 13. From finite-element modeling, we identify this mode as a fundamental quasi-TM WG mode, typically denoted as $WGH_{14,0,0}$, with 96% of the electric field energy in the axial z direction in sapphire; thus it strongly couples to the dipole probe, which is oriented in the axial z direction. The mode displays features consistent with the dipole antiresonance tuning, with the additional feature of a complete mode inversion when the sapphire mode is positioned on resonance with respect to the background mode, similar to electromagnetically induced transparency [20]. This inversion point is also a point of maximum symmetry but, however, has a reduced magnitude of contrast.

A third mode investigated is a fundamental quasi-TM WG mode, typically denoted as $WGH_{11,0,0}$, with 93% of the electric field energy in the axial z direction in sapphire and displaying similar properties to the previous one.

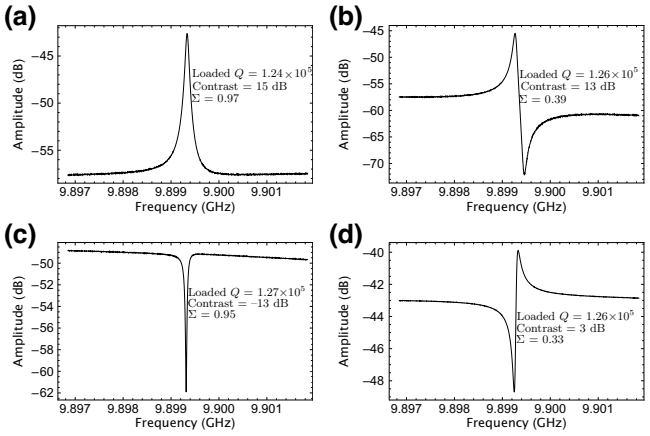

FIG. 13. The 9.899-GHz sapphire mode interacting with a background mode, (a) centered on the antiresonance, (b) with the antiresonance to the right of the mode, (c) centered on the background resonance, and (d) with the antiresonance to the left of the sapphire mode. The loaded Q, contrast, and symmetry values (Σ) are presented for each antiresonance position.

VIII. CONCLUSIONS

In this paper, two techniques of tuning antiresonances within a microwave cavity system have been investigated, including a Mach-Zehnder configuration to excite microwave cavities with a generalized dipole-antenna configuration. The centering of coupled background antiresonances onto the modes of interest produces large improvements in mode symmetry and contrast. These features are desirable in many applications, such as oscillator phase-noise performance.

ACKNOWLEDGMENTS

This work was funded by the Australian Research Council Centre of Excellence for Engineered Quantum Systems (Grant No. CE170100009) and the Australian Research Council Centre of Excellence for Dark Matter Particle Physics (Grant No. CE200100008). We thank Misty Lakelin for contributing the dipole-antenna diagram in Fig. 3.

[1] M. Nagel, S. R. Parker, E. V. Kovalchuk, P. L. Stanwix, J. G. Hartnett, E. N. Ivanov, A. Peters, and M. E. Tobar, Direct terrestrial test of Lorentz symmetry in electrodynamics to 10^{-18}, Nat. Commun. **6**, 8174 (2015).

[2] A. Lo, P. Haslinger, E. Mizrachi, L. Anderegg, H. Müller, M. Hohensee, M. Goryachev, and M. E. Tobar, Acoustic tests of Lorentz symmetry using quartz oscillators, Phys. Rev. X **6**, 011018 (2016).

[3] M. Goryachev, Z. Kuang, E. N. Ivanov, P. Haslinger, H. Muller, and M. E. Tobar, Next generation of phonon tests of Lorentz invariance using quartz BAW resonators, IEEE Trans. Ultrason. Ferroelectr. Freq. Control **65**, 991 (2018).

[4] W. M. Campbell, B. T. McAllister, M. Goryachev, E. N. Ivanov, and M. E. Tobar, Searching for scalar dark matter via coupling to fundamental constants with photonic, atomic, and mechanical oscillators, Phys. Rev. Lett. **126**, 071301 (2021).

[5] C. A. Thomson, B. T. McAllister, M. Goryachev, E. N. Ivanov, and M. E. Tobar, Upconversion loop oscillator axion detection experiment: A precision frequency interferometric axion dark matter search with a cylindrical microwave cavity, Phys. Rev. Lett. **126**, 081803 (2021). [Erratum: Phys. Rev. Lett. 127, 019901 (2021)].

[6] C. A. Thomson, M. Goryachev, B. T. McAllister, E. N. Ivanov, P. Altin, and M. E. Tobar, Searching for low-mass axions using resonant upconversion, Phys. Rev. D **107**, 112003 (2023).

[7] E. Ivanov and M. Tobar, Low noise microwaves for testing fundamental physics. arXiv:2102.11065.

[8] E. N. Ivanov and M. E. Tobar, Microwave phase detection at the level of 10^{-11} rad, Rev. Sci. Instrum. **80**, 044701 (2009).

[9] J. Emmerich and H. Rudolph, The importance of crystal oscillators with low phase noise, Microw. J. **66** (2023).

[10] R. A. Woode, M. E. Tobar, E. N. Ivanov, and D. G. Blair, An ultralow noise microwave oscillator based on a high-Q liquid nitrogen cooled sapphire resonator, IEEE Trans. Ultrason. Ferroelectr. Freq. Control **43**, 936 (1996).

[11] C. R. Locke, E. N. Ivanov, J. G. Hartnett, P. L. Stanwix, and M. E. Tobar, Invited Article: Design techniques and noise properties of ultrastable cryogenically cooled sapphire-dielectric resonator oscillators, Rev. Sci. Instrum. **79**, 051301 (2008).

[12] D. Chaudy, O. Llopis, B. Marcilhac, Y. Lemaître, O. d'Allivy Kelly, J.-M. Hode, and J.-M. Lesage, A low phase noise all cryogenic microwave oscillator based on a superconductor resonator, IEEE Trans. Ultrason. Ferroelectr. Freq. Control **67**, 2750 (2020).

[13] C. Fluhr, B. Dubois, G. Le Tetu, V. Soumann, J. Paris, E. Rubiola, and V. Giordano, Reliability and reproducibility of the cryogenic sapphire oscillator technology, IEEE Trans. Instrument. Measure. **72**, 1 (2023).

[14] M. E. Tobar, E. N. Ivanov, R. A. Woode, J. H. Searls, and A. G. Mann, Low noise 9-gHz sapphire resonator-oscillator with thermoelectric temperature stabilization at 300 kelvin, IEEE Microw. Guided Wave Lett. **5**, 108 (1995).

[15] E. N. Ivanov, M. E. Tobar, and R. A. Woode, Microwave interferometry: Application to precision measurements and noise reduction techniques, IEEE Trans. Ultrason. Ferroelectr. Freq. Control **45**, 1526 (1998).

[16] E. N. Ivanov and M. E. Tobar, Low phase-noise microwave oscillators with interferometric signal processing, IEEE. Trans. Microw. Theory Tech. **54**, 3284 (2006).

[17] E. N. Ivanov and M. E. Tobar, Low phase-noise sapphire crystal microwave oscillators: Current status, IEEE Trans. Ultrason. Ferroelectr. Freq. Control **56**, 263 (2009).

[18] E. N. Ivanov and M. E. Tobar, Noise suppression with cryogenic resonators, IEEE Microw. Wirel. Compon. Lett. **31**, 405 (2021).

[19] U. Fano, Effects of configuration interaction on intensities and phase shifts, Phys. Rev. **124**, 1866 (1961).

[20] M. E. Tobar and D. G. Blair, A generalized equivalent circuit applied to a tunable sapphire-loaded superconducting cavity, IEEE Trans. Microw. Theory Tech. **39**, 1582 (1991).

[21] C. Sames, H. Chibani, C. Hamsen, P. A. Altin, T. Wilk, and G. Rempe, Antiresonance phase shift in strongly coupled cavity QED, Phys. Rev. Lett. **112**, 043601 (2014).

[22] M. Harder, P. Hyde, L. Bai, C. Match, and C.-M. Hu, Spin dynamical phase and antiresonance in a strongly coupled magnon-photon system, Phys. Rev. B **94**, 054403 (2016).

[23] M. Abgrall, J. Guéna, M. Lours, G. Santarelli, M. E. Tobar, S. Bize, S. Grop, B. Dubois, Ch. Fluhr, and V. Giordano, High-stability comparison of atomic fountains using two different cryogenic oscillators, IEEE Trans. Ultrason. Ferroelectr. Freq. Control **63**, 1198 (2016).

[24] M. Born and E. Wolf, *Principles of optics: Electromagnetic theory of propagation, interference, and diffraction of light (7th (expanded) 60th anniversary ed.)* (Cambridge University Press, 2019).

[25] E. N. Ivanov and M. E. Tobar, Frequency stable microwave sapphire oscillators, IEEE Microw. Wirel. Technol. Lett. **33**, 1642 (2023).

[26] J.-J Laurin, Z. Ouardhiri, and J. Colinas, in *2001 IEEE EMC International Symposium. Symposium Record.*

International Symposium on Electromagnetic Compatibility (Cat. No. 01CH37161) (IEEE, 2001), Vol. 1, p. 368.

[27] D. Baudry, C. Arcambal, A. Louis, B. Mazari, and P. Eudeline, Applications of the near-field techniques in EMC investigations, IEEE Trans. Electromag. Compat. **49**, 485 (2007).

[28] Q.-H. Yang, L.-S. Wu, Z.-L. Xu, and J.-F. Mao, A dual-component electric probe embedded with a 0°/180° hybrid coupler for near-field scanning, IEEE Trans. Microw. Theory Tech. **71**, 1112 (2022).

[29] T. E. Tice and J. H. Richmond, Probes for microwave near-field measurements, IRE Trans. Microw. Theory Tech. **3**, 32 (1955).

[30] M. E. Tobar, R. Y. Chiao, and M. Goryachev, Active electric dipole energy sources: Transduction via electric scalar and vector potentials, Sensors **22**, 7029 (2022).

[31] X. Zhang, A. Galda, X. Han, D. Jin, and V. M. Vinokur, Broadband nonreciprocity enabled by strong coupling of magnons and microwave photons, Phys. Rev. Appl. **13**, 044039 (2020).

[32] J. Bourhill, W. Yu, V. Vlaminck, G. E. W. Bauer, G. Ruoso, and V. Castel, Generation of circulating cavity magnon polaritons, Phys. Rev. Appl. **19**, 014030 (2023).

[33] J. W. Rao, C. H. Yu, Y. T. Zhao, Y. S. Gui, X. L. Fan, D. S. Xue, and C.-M. Hu, Level attraction and level repulsion of magnon coupled with a cavity anti-resonance, New J. Phys. **21**, 065001 (2019).